Commun. Comput. Phys.
doi: 10.4208/cicp.321011.020212s

Vol. **13**, No. 3, pp. 696-705
March 2013

Simulations of Boiling Systems Using a Lattice Boltzmann Method

L. Biferale[1,2,*], P. Perlekar[2], M. Sbragaglia[1] and F. Toschi[2]

[1] *Department of Physics and INFN, University of Tor Vergata, Via della Ricerca Scientifica 1, 00133 Rome, Italy.*
[2] *Department of Physics and Department of Mathematics and Computer Science, Eindhoven University of Technology, 5600 MB Eindhoven, The Netherlands.*

Received 31 October 2011; Accepted (in revised version) 2 February 2012

Available online 29 August 2012

Abstract. We report about a numerical algorithm based on the lattice Boltzmann method and its applications for simulations of turbulent convection in multi-phase flows. We discuss the issue of 'latent heat' definition using a thermodynamically consistent pseudo-potential on the lattice. We present results of numerical simulations in 3D with and without boiling, showing the distribution of pressure, density and temperature fluctuations inside a convective cell.

PACS: 47.20.Bp, 47.11.Qr, 47.27.-i, 47.55.-t

Key words: Lattice Boltzmann equation, boiling, thermal convection.

1 Introduction

Thermal convection, the state of a fluid heated from below and cooled from above, is a ubiquitous phenomenon in nature, present in many industrial, geophysical and astrophysical systems [1]. It is also challenging from the theoretical point of view, due to its extremely rich and different regimes, ranging from intricate pattern formations at moderate temperature jumps from bottom and top plates (i.e. moderate Rayleigh number), to extremely turbulent behaviour where heat transfer and its adimensional definition (i.e. Nusselt number) is dominated by bulk or boundary layer physics (or by both, see e.g. recent reviews [2]). Thermal convection is often studied in its simplest version, the so-called Oberbeck-Boussinesq (OB) approximation, where a single phase – unstratified – fluid is present with constant material properties. Compressibility is also neglected except for buoyancy forces. In many situations some, or all, of the above assumptions breaks down

*Corresponding author. *Email address:* biferale@roma2.infn.it (L. Biferale)

and one speaks about Non-Oberbeck-Boussinesq (NOB) convection. Deviations from OB can arise in many different ways. Two notable cases are (i) the presence of stratification (and/or rotation) arising in many geophysical applications and/or (ii) the presence of boiling, i.e. when the parameter excursions inside the convective cell allows for phase transition inside the flow [3–5].

The equations governing the system are the usual – compressible – Navier-Stokes equations supplied with an equation for the internal energy and for an Equation of State (EoS) defining the non-ideal properties at equilibrium:

$$\begin{cases} \partial_t \rho + \partial_j(\rho u_j) = 0, \\ \partial_t \rho u_i + \partial_j(\rho u_i u_j) = -\partial_i P + \partial_j(\mu(\partial_i u_j + \partial_j u_i)) + g\rho\hat{z}, \end{cases} \tag{1.1}$$

where $\mu = \rho\nu$ is the molecular viscosity, g is the gravity, ρ is the local fluid density and

$$P(\rho,T) = P_0(\rho,T) + P_{NI}(\rho)$$

is the non-ideal pressure. Pressure is fixed by the equation of state and it is made of two terms, the ideal part $P_0(\rho,T) = \rho T$ and the non ideal part which in our LBM system reads: $P_{NI}(\rho) = Gexp(-2/\rho)$ (see below). The equation for the internal energy, $U = c_v T + \int d\rho P_{NI}/\rho^2$ is given by:

$$\rho D_t U + P\partial_j u_j = \kappa \partial_{jj} T, \tag{1.2}$$

where κ is the thermal conductivity. The above equation can also be rewritten in terms of the system temperature in two equivalent ways:

$$\begin{cases} c_p \rho D_t T - \alpha T D_t P = \kappa \partial_{jj} T, \\ c_v \rho D_t T + P_0 \partial_j u_j = \kappa \partial_{jj} T, \end{cases} \tag{1.3}$$

where D_t stands for the material derivative, c_v is the specific heat at constant volume, c_p and $\alpha = -(\partial_T \rho)/\rho$ are the specific heat and compressibility at constant pressure, respectively. The above set of equations tends to the usual OB system when the fluid is considered single phase and incompressible, $\rho = const.$, $\partial_j u_j = 0$ and both μ,κ are constant [6]. In this proceedings, we report about some technical issues on how to implement the above set of equations using a Lattice Boltzmann Method and on some preliminary applications to study 3D convection under boiling, i.e. allowing for bubbles nucleation and evaporations inside the convective cell.

2 The LB algorithm

In the non ideal gas lattice Boltzmann model, the force experienced by the particles at $\boldsymbol{x}$ from the particles at $\boldsymbol{x}'$ is assumed to be in the following form [7,8,19]:

$$\boldsymbol{F}(\boldsymbol{x},\boldsymbol{x}') = \mathcal{G}(|\boldsymbol{x}-\boldsymbol{x}'|)\psi(\boldsymbol{x})\psi(\boldsymbol{x}'), \tag{2.1}$$

where $\boldsymbol{x}$ is a function of the local properties at $\boldsymbol{x}$ only. The function $\psi(\boldsymbol{x})$ may be though as an 'effective mass' in the system and is encoding non ideal details of the interactions. For fast-decaying forces, when the sites interacting with the particles on $\boldsymbol{x}$ are limited to their N neighbors, not necessarily the nearest ones, the total force exerted on particles at $\boldsymbol{x}$ is given by summing over all $\boldsymbol{x}'$. Therefore, given a limited set of links that we define as $\boldsymbol{c}_l$, in principle not necessarily the same as those involved in the lattice Boltzmann dynamics, and requiring that the interaction is isotropic (i.e. that $|\boldsymbol{x}-\boldsymbol{x}'|=|\boldsymbol{c}_l|$ brings the same interaction strength) we write

$$\boldsymbol{F}=-\mathcal{G}\psi(\boldsymbol{x})\sum_{l=1}^{N}w(|\boldsymbol{c}_l|^2)\psi(\boldsymbol{x}+\boldsymbol{c}_l)\boldsymbol{c}_l, \tag{2.2}$$

where now $\mathcal{G}$ is a constant of proportionality dictating the overall strength of these non ideal interactions ($\mathcal{G}<0$ encoding attractive interactions). Such form has been used with various choices of ψ by many authors over the last 20 years. Nevertheless, looking at a continuum case where the detail of the interaction is given by a pairwise potential as a function of the distance between two particles, one would be tempted to assume $\psi(\boldsymbol{x})\approx\rho(\boldsymbol{x})$.

Let us now discuss thermodynamical properties following [19]. We take an isothermal system and connect the interaction forces $\boldsymbol{F}$ to the pressure tensor by requiring that the relation

$$\boldsymbol{F}=-\mathcal{G}\psi(\boldsymbol{x})\sum_{l=1}^{N}w(|\boldsymbol{c}_l|^2)\psi(\boldsymbol{x}+\boldsymbol{c}_l)\boldsymbol{c}_l=-\boldsymbol{\nabla}P \tag{2.3}$$

is satisfied exactly on the lattice. To this aim, considering the various force vectors $-\mathcal{G}w(|\boldsymbol{c}_l|^2)\psi(\boldsymbol{x})\psi(\boldsymbol{x}+\boldsymbol{c}_l)$, we can compute their flux over the unit area and immediately derive the pressure tensor summing over all possible interaction links [12]. For example, for nearest neighbor interactions we get

$$\boldsymbol{P}=P_{id}\boldsymbol{\delta}+\frac{\mathcal{G}}{2}\psi(\boldsymbol{x})\sum_{l}w(|\boldsymbol{c}_l|^2)\psi(\boldsymbol{x}+\boldsymbol{c}_l)\boldsymbol{c}_l\boldsymbol{c}_l, \tag{2.4}$$

where $\boldsymbol{\delta}$ is the unit tensor and $P_{id}=\rho T$ is the ideal pressure contribution. When next to nearest neighbor interactions are included, the analytical details are a bit more complicated, but expressions similar to (2.4) are still obtained [12] and they are *exact* on the lattice.

Being exact on the lattice and dealing with a lattice model, we take therefore equation (2.4) as a starting point. If we describe a one dimensional interface developing along z, we can set P_{zz} equal to a constant, say P_0, and determine the interface properties. An expansion of P_{zz} up to second order derivatives [12, 19] delivers

$$P_{zz}^{latt}=P_b(\rho,T)+\frac{\mathcal{G}}{12}\left[a\left(\frac{\partial\psi}{\partial z}\right)^2+b\psi\frac{\partial^2\psi}{\partial z^2}\right]=P_0, \tag{2.5}$$

where $P_b(\rho,T)=\rho T+\frac{\mathcal{G}\psi^2}{2}$ is the bulk pressure and

$$a=1-3e_4, \qquad b=1+6e_4.$$

In the above, e_4 refers to the fourth order tensors associated with the weights $w(|\boldsymbol{c}_l|^2)$, i.e.

$$e_4=\frac{w_1}{2}+2w_2+8w_4+25w_5+32w_8+\cdots.$$

Without losing generality, we have normalized the second order tensor e_2 (that should appear in from of the term $\frac{\mathcal{G}}{2}\psi^2$ in (2.5)) to unity

$$e_2=2w_1+4w_2+8w_4+20w_5+16w_8+\cdots=1.$$

For example, in the case of nearest-neighbor interactions on a square lattice, i.e. $w(|\boldsymbol{c}_l|^2)=0$ for $|\boldsymbol{c}_l|^2>2$, the isotropic conditions up to the forth order tensors determine the two weights as

$$w_1=\frac{1}{3}, \qquad w_2=\frac{1}{12}, \qquad e_4=\frac{1}{3}.$$

If we use the relation

$$\frac{\partial^2\psi}{\partial z^2}=\frac{1}{2}\frac{\partial}{\partial\psi}\left(\frac{\partial\psi}{\partial z}\right)^2$$

we can integrate Eq. (2.5) to obtain

$$\frac{\psi^{1+\epsilon}}{\psi'}\frac{\partial}{\partial\rho}\left[\frac{\mathcal{G}(\psi')^2(\partial_z\rho)^2}{8(1-\epsilon)\psi^\epsilon}\right]=P_0-P_b(\rho,T) \tag{2.6}$$

with

$$\epsilon=-\frac{2a}{b}=\frac{6e_4-2}{6e_4+1}. \tag{2.7}$$

A direct consequence of Eq. (2.6) is that

$$\frac{\mathcal{G}(\psi')^2(\partial_z\rho)^2}{8(1-\epsilon)\psi^\epsilon}=\int_{\rho_g}^{\rho}(P_0-P_b(\xi,T))\frac{\psi'}{\psi^{1+\epsilon}}d\xi.$$

Since in the liquid bulk phase we have that $(\partial_z\rho)^2=0$, we therefore end up with an integral constraint such that [19]:

$$\int_{\rho_g}^{\rho_l}(P_0-P_b(\rho,T))\frac{\psi'}{\psi^{1+\epsilon}}d\rho=0. \tag{2.8}$$

An alternative to Eq. (2.8) comes from considering the *continuum* pressure tensor, instead of the lattice one reported in (2.4). Such continuum pressure tensor is obtained from (2.3) by taking the Taylor expansion of the force field

$$\boldsymbol{F}=-\mathcal{G}\psi(\boldsymbol{x})\sum_{l=1}^{N}w(|\boldsymbol{c}_l|^2)\psi(\boldsymbol{x}+\boldsymbol{c}_l)\boldsymbol{c}_l\approx-\mathcal{G}\psi(\boldsymbol{x})\boldsymbol{\nabla}\psi(\boldsymbol{x})+\cdots$$

and then satisfying (2.3) up to second order in such Taylor expansion [13]. Skipping all the technical steps (they can be found in [13]), we report directly the result for the integral constraint imposing the mechanical equilibrium

$$\int_{\rho_g}^{\rho_l} (P_0 - P_b(\rho,T)) \frac{\psi'}{\psi^2} d\rho = 0 \tag{2.9}$$

that now is independent of ϵ.

2.1 Numerical benchmarks

We now proceed to a numerical benchmark, using the pseudopotentials $\psi(\rho)=e^{-1/\rho}$ and $\psi(\rho)=1-e^{-\rho}$. We then choose nearest neighbor interactions, so that $\epsilon=0$. In Fig. 1 we report equilibrium densities as a function of the temperature T. We choose $w_1=\frac{1}{3}$, $w_2=\frac{1}{12}$ and $w_i=0$ $(i\geq 2)$, corresponding to $\epsilon=0$. We then consider a one dimensional interface at constant pressure P_0, and report the liquid and gas densities as obtained with lattice Boltzmann simulations with $\psi(\rho)=e^{-1/\rho}$ (left panel) and $\psi(\rho)=1-e^{-\rho}$ (right panel). The coupling strength in (2.2) has been chosen equal to $\mathcal{G}=-\frac{4}{3}$. The theoretical prediction for the two cases has been obtained from the integral constraint (2.8) and is reported with the black solid line. As we can see, the agreement between the theory and numerical is very good.

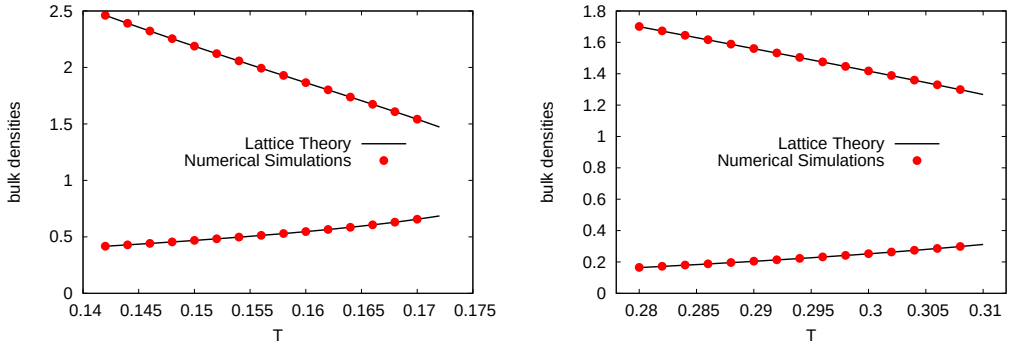

Figure 1: The equilibrium densities as a function of the temperature T. For the same value of $\epsilon=0$, we consider a one dimensional interface at constant pressure P_0, and report the liquid and gas densities as obtained with lattice Boltzmann simulations with $\psi(\rho)=e^{-1/\rho}$ (left panel) and $\psi(\rho)=1-e^{-\rho}$ (right panel). The theoretical prediction for the two cases has been obtained from the integral constraint $\int_{\rho_g}^{\rho_l}(P_0-\rho T-\frac{\mathcal{G}}{2}\psi^2)\frac{\psi'}{\psi}d\rho=0$ and is reported with the black solid line.

Next we proceed to test the prediction of Eq. (2.9). In Fig. 2 we report the numerical data previously discussed for the case with $\psi(\rho)=1-e^{-\rho}$. As we can see, the lattice argument is working better than the continuum counterpart.

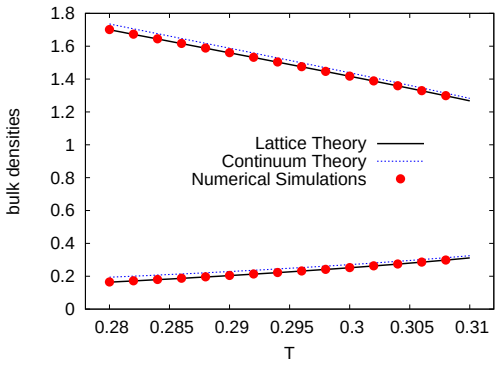

Figure 2: The equilibrium densities as a function of the temperature T. For the same value of $\epsilon=0$, we consider a one dimensional interface at constant pressure P_0, and report the liquid and gas densities as obtained with lattice Boltzmann simulations with $\psi(\rho)=1-e^{-\rho}$. Both the theoretical predictions reported in (2.8) and (2.9) are reported.

3 Clausius Clapeyron relation

It is now instructive to show the difference between data reported in Fig. 1 in terms of equilibrium thermodynamics. We have seen that the integral constraint coming from the lattice theory (2.8) is able to predict very well the equilibrium densities for both the pseudopotentials $\psi(\rho)=1-e^{-\rho}$ and $\psi(\rho)=e^{-1/\rho}$. The crucial difference between the two cases is that the pseudopotential $\psi(\rho)=e^{-1/\rho}$ leads to an integral weight in (2.8) that is the very same predicted by Maxwell rule

$$\frac{\psi'}{\psi}=\frac{1}{\rho^2}, \quad \text{for} \quad \psi(\rho)=e^{-1/\rho}, \tag{3.1}$$

something that is not possible for the pseudopotential $\psi(\rho)=1-e^{-\rho}$. We therefore argue that the pseudopotential $\psi(\rho)=e^{-1/\rho}$ leads to a consistent thermodynamic description. In other words, in case of $\psi(\rho)=e^{-1/\rho}$ we should be able to define a chemical potential and set it to the same bulk values at equilibrium. The latter condition leads directly to the well known Clausius Clapeyron equation

$$\frac{dP}{dT}=\frac{\Delta s}{\Delta v} \tag{3.2}$$

which we can verify in the numerics. In the above, P is the equilibrium pressure at coexistence temperature T, $v=1/\rho$ is the specific volume, and

$$s(T,\rho)=-\log\left(\frac{\rho}{T^{D/2}}\right)$$

is the specific entropy. We note that the functional form of the entropy is the same as that of an ideal gas, the reason being that the potential interactions (2.1) are built with interaction tails and therefore we expect no influence on the entropy function (at least that's

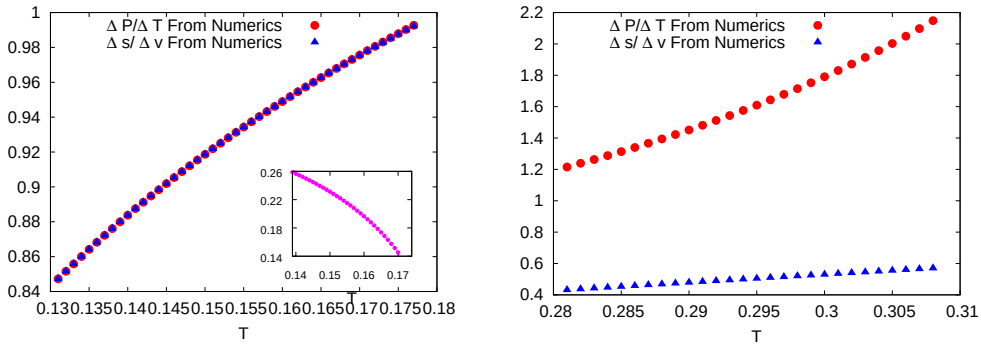

Figure 3: We report the evaluation of the terms dP/dT and $\Delta s/\Delta v$ as computed from the equilibrium data reported in Fig. 1. In the previous notation, P is the equilibrium pressure at coexistence temperature T, $v=1/\rho$ is the specific volume, and $s(T,\rho)=-\log\left(\frac{\rho}{T^{D/2}}\right)$ is the specific entropy. Clausius Clapeyron relation predicts the equality of both terms. In the left panel data obtained with the pseudopotential $\psi=e^{-1/\rho}$ show thermodynamical consistency. The inset shows the latent heat extracted from $\lambda=T\Delta s$. The right panel corresponds to data obtained with the pseudopotential $\psi=1-e^{-\rho}$ and are not thermodynamically consistent.

the lesson learned from the Van Der Waals model, where the entropy is solely influenced by the local exclusion volume effect). As we see from the left panel of Fig. 3, the terms dP/dT and $\Delta s/\Delta v$ in (3.2) match very well when computed from the equilibrium data from Fig. 1. The same does not happen for equilibrium data coming from the pseudopotential $\psi(\rho)=1-e^{-\rho}$ (right panel of Fig. 3). With the matching of both terms in (3.2) we are therefore able to couple in a consistent way the heat associated with phase transition (embedded in Δs) with the mechanical part of the model (embedded in P). This offers a direct natural link with the latent heat

$$\lambda(T)=T\Delta s. \tag{3.3}$$

which, in our case, corresponds to the inset of the left panel of Fig. 3. A numerical fit leads to the following expression in the range $0.14\leq T\leq 0.17$

$$\lambda(T)=-0.845166+17.2615T-67.2153T^2.$$

3.1 LBM implementation and results

Despite the existence of fully thermal lattice Boltzmann schemes [9], also applied to high Reynolds and Rayleigh systems [10, 11], we prefer here to adopt a standard two populations lattice Boltzmann models (LBM) [14]. The main reason is that thermal algorithms need long-range velocity speeds on the lattice leading to highly non-trivial spurious effects at the boundaries. Here, being interested in thermal convection, a system fully driven by thermal instabilities at the boundaries, we need to have the physics of the boundary layer better under control. The starting point is a standard coupled mesoscopic

dynamics described by [14,15]:

$$f_l(\boldsymbol{x}+\boldsymbol{c}_l,t+1)-f_l(\boldsymbol{x},t)=-\frac{1}{\tau}(f_l-f_l^{(eq)})(\boldsymbol{x},t), \tag{3.4a}$$

$$g_l(\boldsymbol{x}+\boldsymbol{c}_l,t+1)-g_l(\boldsymbol{x},t)=-\frac{1}{\tau_g}(g_l-g_l^{(eq)})(\boldsymbol{x},t), \tag{3.4b}$$

where $f_l(\boldsymbol{u},t)$, $g_l(\boldsymbol{x},t)$ stand for the probability density functions to find at $(\boldsymbol{x},t)$ a particle whose kinetic velocity belongs to a discrete and limited set $\boldsymbol{c}_l$ (with $l=0,18$ in the $D3Q19$ LBM adopted here [14]). Hydrodynamical fields, density, momentum and temperature are defined as coarse-grained quantities of the distribution functions

$$\rho=\sum_l f_l, \qquad \rho\boldsymbol{u}=\sum_l \boldsymbol{c}_l f_l, \qquad T=\sum_l g_l. \tag{3.5}$$

A Chapman-Enskog expansion [16] around the local equilibria

$$f_l^{(eq)}(\boldsymbol{u}',\rho,T)=w_l\left[\rho S_l(T)+\frac{\rho u_k' c_l^k}{c_s^2}+\frac{(c_l^k c_l^s-c_s^2\delta_{ks})(\rho u_k' u_s')}{2c_s^4}\right],$$

$$g_l^{(eq)}(\boldsymbol{u}^{(H)},T)=w_l T\left[1+\frac{u_k^{(H)}c_l^k}{c_s^2}+\frac{(c_l^k c_l^s-c_s^2\delta_{ks})(u_k^{(H)}u_s^{(H)})}{2c_s^4}\right]$$

leads to the equations for density, momentum and temperature (1.1)-(1.3), with $\nu=c_s^2(\tau-1/2)$ and $\kappa=c_s^2(\tau_g-1/2)$ [14]. In the above equations, the hydrodynamical velocity is defined as $\boldsymbol{u}^{(H)}=\boldsymbol{u}+\frac{1}{2}\frac{\boldsymbol{F}}{\rho}$, while the primed velocity is such that $\boldsymbol{u}'=\boldsymbol{u}+\frac{\tau\boldsymbol{F}}{\rho}$. Lattice discrete effects in the introduction of the forcing term are then controlled with the ideas proposed in [16]. Notice that in order to reproduce the correct ideal part of the pressure, $P_0=\rho T$, a coupling between f_l and g_l populations in (1.3) is introduced using a recent proposal by Zhang and Tian [17] by plugging the dynamical temperature in the equilibrium distribution of (3.4a). This is the reason for the presence of the extra term $S_l(T)=3T$ ($l=1,\cdots,18$), $S_0(T)=3-6T$. In order to reproduce exactly the divergence term, $P_0\partial_j u_j$, in (1.3), we also found necessary to add a proper counter term to the evolution of g_l populations in (3.4b), similarly to what has been done in [18]. The idea is to add a isotropic volume term in the RHS of (3.4b) projecting only on the zero-th order manifold without affecting higher order momenta. Moreover, adopting the definition of the temperature as in (3.5), we found necessary to add the extra diffusive term $\kappa(\frac{1}{\rho}-1)\Delta T$ to get Eq. (1.3).

As a result, we ended with a LBM scheme able to reproduce in the hydrodynamic limit the NS equations (1.1)-(1.3) with a non-ideal Pressure tensor and a consistent definition of latent heat. See Fig. 4 for a plot of the compressibility at constant pressure $\alpha=-(\partial_T\rho)/\rho$ and at constant temperature $\beta=\partial_P\rho/\rho$ calculated in the two phase coexistence regime for the boiling simulation and in the non boiling case. In Fig. 5 we have shown a scatter plot of phase diagrams for a boiling cell. As one can see most of the

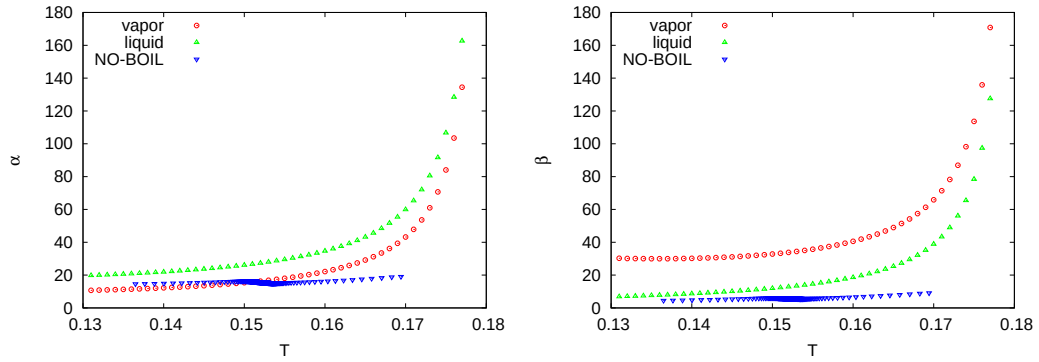

Figure 4: Compressibility at constant pressure (left) and constant temperature (right) defined in the liquid or vapor phase for boiling simulations or for the single-phase liquid.

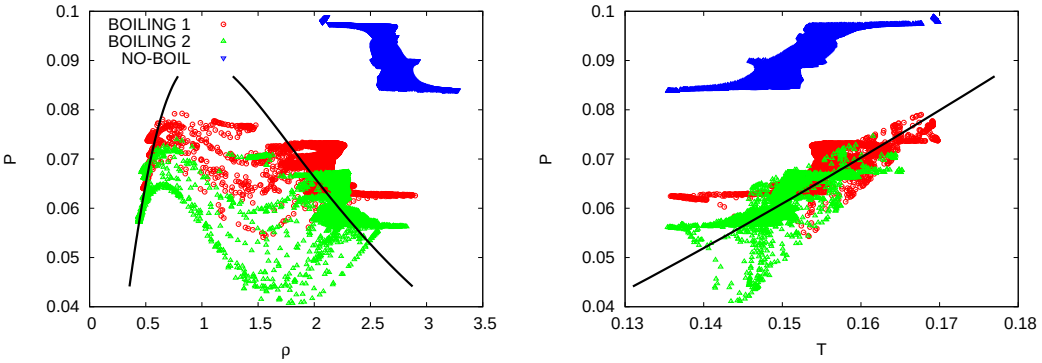

Figure 5: Thermodynamic properties inside the convective cell for three different simulations. Two simulations with phase-coexistence (BOILING 1 and 2) and one simulation with single phase liquid (NO-BOILING).

volume is at *thermodynamical equilibrium*, superposing with the equilibrium curves in the $T-\rho$ phase space. The presence of bubbles is clearly detected by the spots concentrating along the $\rho=\rho_g$ branch and it is also interesting to notice that the corresponding bubble temperature is always larger than the mean temperature in the cell, indicating that bubbles are transferring temperature upwards very efficiently [20].

Acknowledgments

The authors would like to thank R. Verzicco and H. Chen for useful discussions.

References

[1] P. Cardin & P. Olson, Phys. of The Earth and Planetary Interiors, 82, 235–259 (1994); G.A. Glatzmaier & P. H. Roberts, Nature, 377, 203–209 (1995).

[2] E. Bodenschatz, W. Pesch & G. Ahlers, Annu. Rev. Fluid Mech., 32, 709-778 (2000); G. Ahlers, S. Grossmann & D. Lohse, Rev. Mod. Phys., 81, 503 (2009).
[3] J.-Q. Zhong, D. Funfschilling & G. Ahlers, Phys. Rev. Lett., 102, 124501 (2009).
[4] V.K. Dhir, Annu. Rev. Fluid Mech., 30, 365–401 (1998).
[5] P. Oresta et al., Phys. Rev. E, 80, 026304 (2009).
[6] A. Spiegel & G. Veronis, Astrophys. J., 131, 442 (1960).
[7] X. Shan & H. Chen, Phys. Rev. E, 47, 1815 (1993).
[8] R. Zhang & H. Chen, Phys. Rev. E, 67, 066711 (2003).
[9] M. Sbragaglia et al., J. Fluid Mech., 628, 299 (2009).
[10] L. Biferale et al., Phys. Fluids, 22, 115112 (2011).
[11] L. Biferale et al., Phys. Rev. E, 84, 016305 (2011).
[12] X. Shan, Phys. Rev. E, 77, 066702 (2008).
[13] M. Sbragaglia et al., Phys. Rev. E, 75, 026702 (2007).
[14] S. Succi, The Lattice Boltzmann Equation, Oxford Science, New York, 2001.
[15] J. Latt, PhD Thesis, University of Geneve, 2007.
[16] B. Shi & Z. Guo, Phys. Rev. E, 79, 016701 (2009); Z. Guo, C. Zheng & B. Shi, Phys. Rev. E, 65, 046308 (2002).
[17] J. Zhang & F. Tian, Europhys. Lett., 81, 66005 (2008).
[18] N.I. Prasianakis & I.V. Karlin, Phys. Rev. E, 76, 016702 (2007).
[19] M. Sbragaglia & X. Shan, Phys. Rev. E, 84, 036703 (2011).
[20] L. Biferale, P. Perlekar, M. Sbragalia & F. Toschi, Phys. Rev. Lett, submitted (2011).